

# SPONTANEOUS VIBRATIONS AND STOCHASTIC RESONANCE OF SHORT OLIGOMERIC SPRINGS

Alexey M. Astakhov<sup>1,2,a</sup>, Vladislav S. Petrovskii<sup>1,2,a</sup> , Maria A. Frolkina<sup>1,2</sup> , Anastasia A. Markina<sup>1,2</sup> ,  
Alexander D. Muratov<sup>1,2,b</sup> , Alexander F. Valov<sup>1,2</sup> and Vladik A. Avetisov<sup>1,2,c</sup> 

<sup>1</sup> Semenov Federal Research Center for Chemical Physics, Russian Academy of Sciences, Moscow, Russia

<sup>2</sup> Design Center for Molecular Machines, Moscow, Russia

<sup>a</sup> A.M.A. and V.S.P. contributed equally to this work

<sup>b</sup> alexander.muratov@chph.ras.ru

<sup>c</sup> avetisov@chph.ras.ru

## ABSTRACT

There is growing interest in molecular structures that exhibit dynamics similar to bistable mechanical systems. These structures have the potential to be used as two-state operating units for various functional purposes. Particularly intriguing are the bistable systems that display spontaneous vibrations and stochastic resonance. Previously, through molecular dynamics simulations, it was discovered that short pyridine-furan springs in water, when subjected to stretching with power loads, exhibit the bistable dynamics of a Duffing oscillator. In this study, we extend these simulations to include short pyridine-pyrrole and pyridine-furan springs in a hydrophobic solvent. Our findings demonstrate that these systems also display the bistable dynamics, accompanied by spontaneous vibrations and stochastic resonance activated by thermal noise.

**Keywords** Nanosprings · nonlinear dynamics · bistability · spontaneous vibrations · stochastic resonance · Duffing oscillators

## 1 Introduction

The increasing focus on nanoscale molecular structures with dynamics reminiscent of bistable mechanical systems is driven by the growing demand for designing and implementing various nanodevices. These devices serve as switches and logic gates[1, 2, 3, 4, 5, 6], sensors and actuators[7, 8, 9, 10, 11], mechanoelectrical transducers and energy harvesters[12, 13, 14, 15, 16]. Nanoscale bistable systems are equally crucial for validating the principles of stochastic thermodynamics[17, 18, 19, 20]. This field currently aims to expand thermodynamic theories to encompass nanoscale molecular machines[20, 21, 22, 23, 24].

This article focuses on nanoscale molecular structures whose dynamic prototypes are the textbook bistable mechanical systems known as Euler arches[25, 26] and Duffing oscillators[27, 28]. In particular, using molecular dynamics simulations, it was found that the long-term conformational dynamics of short rod-shaped thermosensitive oligomers were similar to the bistable dynamics of an Euler arch[29, 30], while particular oligomers of a helical form stabilized by weak intermolecular interactions could behave as bistable Duffing oscillators[31].

In general, Euler arches and Duffing oscillators can be perceived as mechanical systems whose potential energy is determined by fourth-degree polynomial function caused with nonlinear elasticity of the system elements. The potential energy of these systems has either one minimum or two energy wells separated by a bistability barrier. Therefore, the system can have different dynamic modes controlled by the power loads applied to the system. In particular, the force load compressing an Euler arch controls the arch dynamics, while the stretching of a Duffing spring controls the spring dynamics. Therefore, with driving the power loads, one can operate by dynamical modes of the system and, accordingly, carry out the transitions between the system discrete states in a controlled manner.

In addition to deterministic transitions, jump-like spontaneous transitions between the two states of a bistable system, known as spontaneous vibrations, can occur due to random disturbances of the system. In the mode of spontaneous vibrations, the time intervals between the jumping (the lifetimes of the system in its states) are random values whose average grows exponentially with increasing ratio of the bistability barrier to the intensity of noise, following Kramer’s rate approximation[32]. Therefore, spontaneous vibrations are actually observed when this ratio is not excessively large, such as when the bistability barrier is approximately an order of magnitude higher than the noise intensity. On the other hand, by applying a gentle oscillating force that rocks the bistable potential, spontaneous vibrations can be transformed into almost regular switching between the two states, induced by noise. This phenomenon is referred to as stochastic resonance[33]. Both spontaneous vibrations and stochastic resonance are remarkable manifestations of bistability.

Stochastic resonance is an intriguing phenomenon that arises from the interplay between the bistable dynamics of a system and its stochastic perturbations. Unlike typical noise effects that tend to blur signals, the noise actually amplifies weak signals in the stochastic resonance regime. While the initial concept of stochastic resonance was proposed to explain the regularity of ice ages on Earth[33, 34, 35], it sparked a proliferation of research exploring its practical applications and interpretations in various macroscopic, global, and even celestial systems[36, 37].

In recent years, experimental evidence has emerged indicating the potential presence of bistable patterns at sub-micron scales, such as in nanotubes[38, 39, 40], graphene sheets[14, 41], DNA hairpins, and proteins[42, 43, 44]. It is worth noting that spontaneous vibrations and stochastic resonance in macroscopic mechanical systems, even those as small as a micron, are unlikely to be triggered solely by environmental thermal noise. The bistability barriers in macroscopic systems are much higher than the intensity of thermal noise ( $\sim k_B T$ ) at natural conditions, necessitating much stronger random perturbations to activate spontaneous vibrations and stochastic resonance, even at the micron scale.

Designing a mechanical system with the nonlinear elasticity inherent in a Duffing oscillator is also a non-trivial task. In mechanics, creative combinations of springs have been devised to mimic the Duffing’s bistability (for an example, refer to Lai and Leng [45], Lu et al. [46]). However, in nanoscale mechanics, a potential solution may arise primarily due to strong nonlinearity of weak intermolecular interactions whose contribution to the potential energy of a nano-size molecular system may appear significant for collective dynamical modes of the system. An equally important perspective comes from the fact that the bistability barriers of nanoscale systems can be high enough to well separate dynamic states against a background of thermal fluctuations, and at the same time low enough for thermal fluctuations to activate transitions between the well-separated states. A ratio of bistability barrier to thermal noise intensity of approximately ten can serve as a reasonable benchmark. Oligomeric molecules a few nanometers in size appear to be potential representatives of target molecular systems.

Notably, recent intensive molecular dynamic simulations investigating short oligomeric compounds subjected to force loads have uncovered bistable molecules that exhibit the dynamic behavior resembling that of the Euler arches and Duffing oscillators[29, 30, 31]. These simulations have revealed the presence of mechanic-like bistability in specific oligomeric molecules, accompanied by spontaneous vibrations and stochastic resonance activated by thermal fluctuations. In this paper we continue our search for bistable nanoscale molecular structures and investigate behaviour of short pyridine-pyrrole (PP) and pyridine-furan (PF) springs in hydrophobic solvent.

## 2 Materials and Methods

### 2.1 Pyridine-Pyrrole and Pyridine-Furan Springs

PP and PF copolymers (Figure 1a) are conductive polymers consisting of 5- and 6-member heterocyclic rings as synthesized and described by Alan Jones et al. [47] and Alan Jones and Covic [48], respectively. These copolymers tend to assume a helix-like shape, which is squeezed by the  $\pi - \pi$  interactions of aromatic groups located at the adjacent turns[49]. Assuming that stacking could lead to nonlinear elasticity of the springs and following the quantum calculations of the stacking energy for different configurations of heterocyclic rings[49], the cis-configuration of oligo-PP and oligo-PF with heteroatoms of the 5- and 6-member heterocyclic rings on one side of a polymer chain was selected (see Figure 1a)). Guided by the preliminary screening of sizes, we designed two spring models consisting of five monomer units (oligo-PP-5 and oligo-PF-5) as shown in Figure 1b,c). Both springs were solvated in hydrophobic solvent, tetrahydrofuran (THF). The distance between the adjacent turns was close to 0.35 nm in all non-stretched samples according to Sahu et al. [49].

### 2.2 Simulation Details

The oligo-PP- and oligo-PF-springs and the environmental solvent were modeled in a fully atomistic representation with a canonical (symbol/volume/temperature [NVT]) ensemble (box size:  $4.5 \times 4.5 \times 4.5 \text{ nm}^3$  for oligo-PP,  $7.0 \times 7.0 \times 7.0 \text{ nm}^3$  for oligo-PF) with a time step of 2 fs using Gromacs 2019[50] and the OPLS-AA[51] force field parameters (for

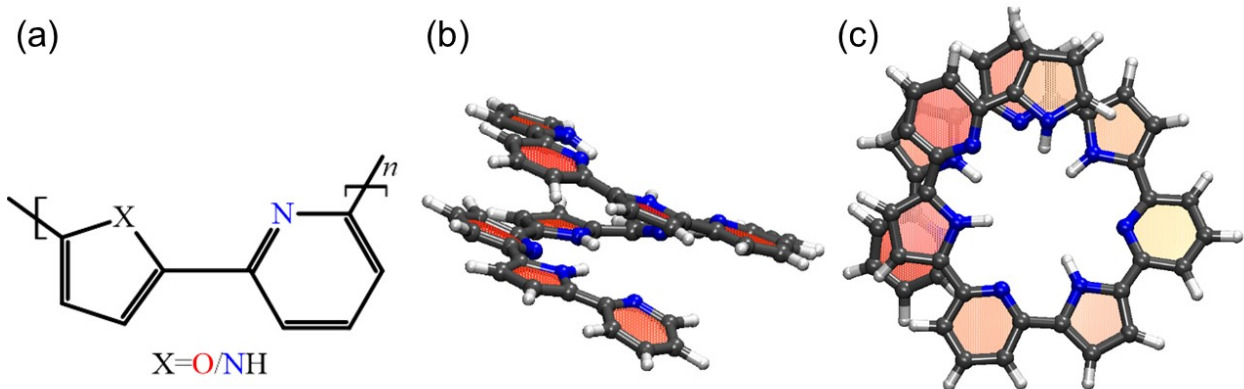


Figure 1: Pyridine–furan (PF) and pyridine–pyrrole (PP) springs with five monomer units (oligo-PF-5 spring and oligo-PP-5 spring, respectively): (a) Chemical structure of a pyridine–furan ( $X$  represents oxygen,  $O$ ) /pyridine–pyrrole monomer ( $X$  represents  $NH$  group) unit with heterocyclic rings in cis-configuration. (b) Front and (c) top views of an oligo-PP-5 spring in the atomistic representation. The spring has one complete turn consisting of approximately 3.5 monomer units.

more details, see Parameters for Molecular Dynamics simulation section of Supporting Information ). The temperature was set at 280 K by the velocity-rescale thermostat[52], which corresponds to the equilibrium state of the springs[49]. Each dynamic trajectory was 300 – 350 ns long and was repeated three times to obtain better statistics; therefore, the effective length of the trajectories was about one  $\mu$ s for each sample.

The dynamics of the springs were studied by fixing one end of the spring, while the other end was pulled by a force applied along the axis of the spring. The distance (denoted  $R_e$ ) between the ends of the spring (yellow and blue balls in Figure 2a)) was considered a collective variable describing the long-term dynamics of the spring. Bistability of the spring was specified in agreement with two well reproduced states of the spring with the end-to-end distances equal to  $R_e \sim 1.10$  nm and  $R_e \sim 1.45$  nm. These states are referred to as the squeezed and the stress-strain states, respectively.

### 3 Results

#### 3.1 Bistable dynamics of oligo-PP-5 spring

To investigate the dynamics of the oligo-PP-5 springs under tension, we initially equilibrated the oligo-PP-5 spring at 280 K with one end fixed. Subsequently, we applied a force  $\vec{F}$  along the spring axis to pull the other end. Under weak tensile conditions, the spring’s initial state, compressed by stacking, remained stable, and the spring underwent slight stretching in accordance with linear elasticity. Note that for oligo-PP-5 spring we measured not the end-to-end distance, but the distance between the pulled end and the monomer that contacts the pulled end in the squeezed state (see comparison in SI). However, when the pulling force reached a specific critical value of approximately  $F_c = 30$  pN, the oligo-PP-5 spring exhibited bistability and commenced to vibrate spontaneously. At the critical force value, a junction point emerged, leading to a split into two branches: the branch of zero-stress attractors, representing a stress-strain state, and the branch of unsteady zero-stress states, repelling the dynamic trajectories.

Simultaneously, the squeezed states remain attractive. From the perspective of nonlinear dynamical systems, the dynamics of the oligo-PP-5 spring bifurcate at the critical force  $F_c = 30$  pN. Beyond this critical tensile point, the spring becomes bistable and exhibits spontaneous vibrations, alternating between the squeezed and stress-strain states. The average end-to-end distances of the spring in the squeezed and stress-strain states differ by approximately 0.35 nm, allowing for clear distinction between these two states. Figure 2a) shows atom level snapshots of these two states. Notably, this difference suggests an extension of the stacking pair length to almost twice its original size. As a result, the  $\pi - \pi$  interactions do not significantly contribute to the elastic energy of the stress-strain states, with the spring’s elasticity mainly determined by the rigidity of the oligomeric backbone.

Figure 2d) illustrates the evolution of the statistics of visits to the squeezed and stress-strain states as the pulling force exceeds the critical point  $F_c$ . Below  $F_c$ , the squeezed state represents the sole steady state of the spring. However, at the bifurcation point  $F_c$ , the stress-strain state emerges, rendering the oligo-PP-5 spring bistable, causing it to spontaneously vibrate, although the squeezed state predominates near the critical point  $F_c$ . At  $F \approx 75$  pN, both the

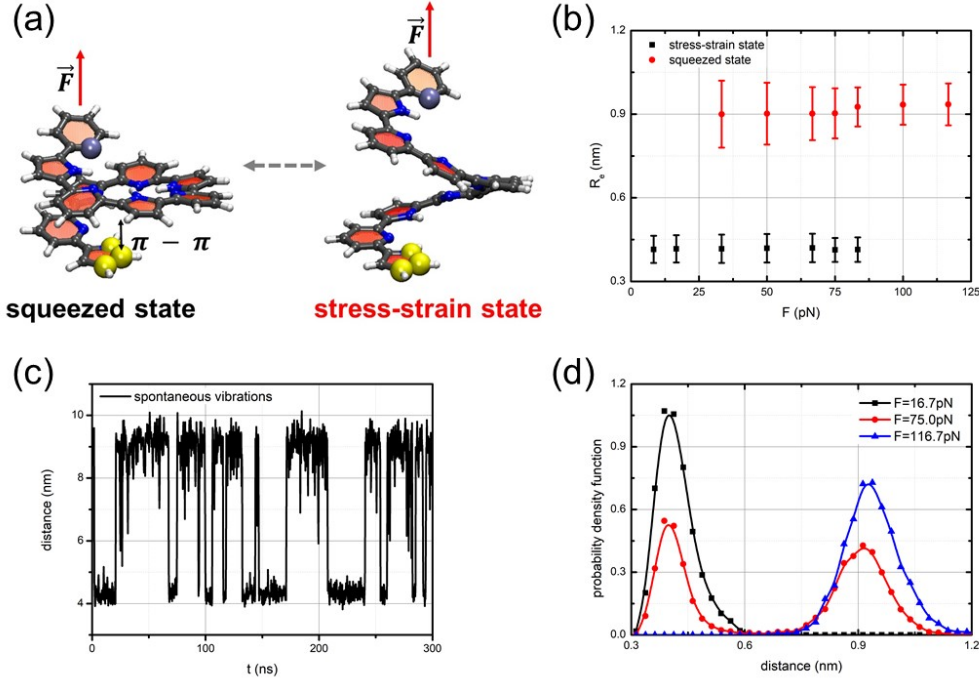


Figure 2: (a) Computational models of the oligo-PP-5 system with applied longitudinal load. The squeezed and the stress-strain states of the spring are shown on the right and left, respectively. The pulling force,  $F$ , is applied to the top end of the spring; (b) The state diagram shows a linear elasticity of oligo-PF-5 spring up to  $F \approx 30$  pN and bistability of the spring in the region from  $F \approx 30 - 80$  pN; (c) Spontaneous vibrations of the oligo-PP-5 spring at  $F \approx 75$  pN; (d) Evolution of the probability density for the squeezed and stress-strain states when pulling force surpasses the critical value.

squeezed and stress-strain states are almost equally visited, signifying that the bistability of the oligo-PP-5 spring becomes approximately symmetrical at a considerable distance from the critical point.

In this region, the spontaneous vibrations of the oligo-PP-5 spring are most pronounced. The mean lifetimes of the squeezed and stress-strain states in the spontaneous vibration mode varied in the bistability region, ranging from  $\tau = 1 - 20$  ns, depending on the pulling force. In the symmetrical bistability region, neither the squeezed state nor the stress-strain state dominates, resulting in the mean lifetimes of the two states being approximately equal to  $\tau = 14$  ns.

Utilizing Kramer's rate approximation with a collision time for random perturbations ranging from  $0.1 - 10$  ps, we can roughly estimate the bistability barrier of the oligo-PP-5 spring as  $\sim 10 k_B T$ . Noteworthy, the bistability barrier of this bistable oligomeric system is approximately ten times greater than the characteristic scale of thermal fluctuations,  $k_B T$ . Figure 2c) displays a typical trajectory of the long-term dynamics  $R_e(t)$  of the oligo-PP-5 spring within the symmetric bistability region. Clear spontaneous vibrations of the spring can be observed without any additional random perturbations applied to activate them. Instead, these vibrations are solely activated by thermal-bath fluctuations. On the other hand, outside the bistability region, non-vibrating trajectories are prevalent.

To investigate the stochastic resonance mode of the oligo-PP-5 spring, we introduced an additional weak oscillating force applied to the pulling end of the spring. This oscillating force was modeled by applying an oscillating electrical field,  $E = E_0 \cos(2\pi\nu t)$ , to a unit charge located on the pulling end of the spring. A counterion was placed at  $2.2$  nm from spring centre of mass on the pull axis to balance the system. We need to note that addition of the charge and a fixed counterion significantly changes the critical force parameters of bistability - for this particular configuration, system exhibits spontaneous vibrations even without additional pulling force, and reaches symmetrical distribution at  $F = 3.5$  pN (for more details, refer to the "Parameters of periodic signal" section in the Supporting Information).

Figure 3a) presents typical vibrations of the end-to-end distance of the oligo-PP-5 spring in the stochastic resonance mode, along with the power spectrum of these vibrations.

After some preliminary analysis, we decided to examine frequency response at oscillating field amplitude  $E_0 = 0.12 \text{ V nm}^{-1}$ , because at amplitudes above  $E_0 > 0.15 \text{ V nm}^{-1}$  system behavior resembled forced oscillations and not

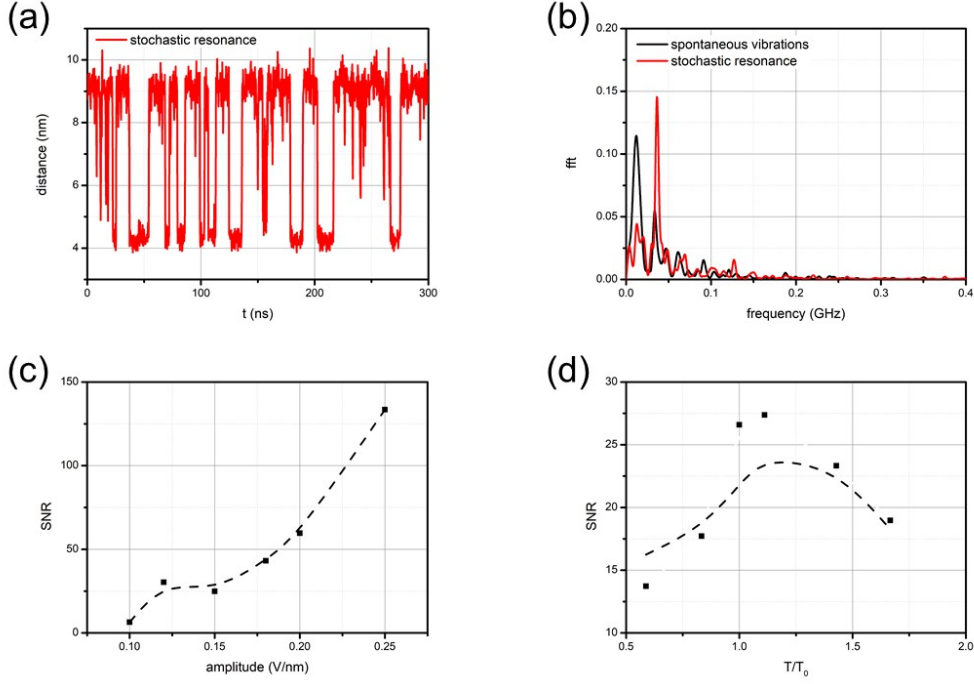


Figure 3: Stochastic resonance of the oligo-PP-5 induced by an oscillating field  $E = E_0 \cos(2\pi\nu t) = E_0 \cos(2\pi t/T)$ : (a) The dynamic trajectory at  $F = 3.5$  pN,  $T = 28$  ns, and  $E_0 = 0.12$  V nm $^{-1}$ ; (b) Power spectrum of spontaneous vibrations (black curve) and stochastic resonance (red curve); (c) The dependence of the main resonance peak amplitude on  $E_0$  ( $T_0 = 28$  ns); (d) The dependence of the main resonance peak amplitude on the period  $T$  of oscillating field ( $E_0 = 0.12$  V nm $^{-1}$ ).

stochastic resonance (mean lifetime in state was directly proportional to external signal period). According to the theory of stochastic resonance [36, 37], the primary resonance peak was observed at a frequency of  $\nu = 1/2\tau$ , where the period of the applied oscillating field was equal to twice the mean lifetime of the states in the spontaneous vibration mode. We extensively scanned a wide range of oscillating fields to identify the maximal resonance response, as determined by the spectral component at the resonance frequency. Figure 3c-d) presents the corresponding results. The maximum resonance response was observed when the period of the oscillating field was close to twice the mean lifetime of the states in the spontaneous vibration mode.

### 3.2 Bistable dynamics of oligo-PF-5 spring

To investigate the dynamics of the oligo-PF-5 springs under tension, we followed the same protocol as for the oligo-PP-5. First, we equilibrated the oligo-PF-5 spring at 280 K with one end fixed. Then, we applied a force  $\vec{F}$  along the spring axis to pull the other end. Once again, under weak tensile conditions, the spring's initial state remained stable, and it underwent slight stretching in line with linear elasticity due to the stacking. However, once the pulling force reached a specific critical value, the oligo-PF-5 spring exhibited bistability and began to exhibit spontaneous vibrations in the same way as the oligo-PP-5. As the pulling force reached the critical value, approximately  $F_c = 50$  pN, a junction point emerged, dividing the system into two branches: one corresponding to the stress-strain state with zero-stress attractors, and the other representing unsteady zero-stress states that repelled dynamic trajectories. Simultaneously, the squeezed states remain attractive. The average end-to-end distances of the spring in the squeezed and stress-strain states differ by approximately 0.35 nm, allowing for clear distinction between these two states. Figure 4a) displays atomic level snapshots of these two states. Notably, this difference suggests an extension of the stacking pair length to almost twice its original size. As a result, the  $\pi - \pi$  interactions do not significantly contribute to the elastic energy of the stress-strain states, with the spring's elasticity mainly determined by the rigidity of the oligomeric backbone.

Figures 4b) and d) illustrate the evolution of the statistics of visits to the squeezed and stress-strain states as the pulling force exceeds the critical point  $F_c$ . Below  $F_c$ , the squeezed state represents the sole steady state of the spring. However, at the bifurcation point  $F_c$ , the stress-strain state emerges, rendering the oligo-PF-5 spring bistable, causing it to spontaneously vibrate, although the squeezed state predominates near the critical point  $F_c$ . Within the range of

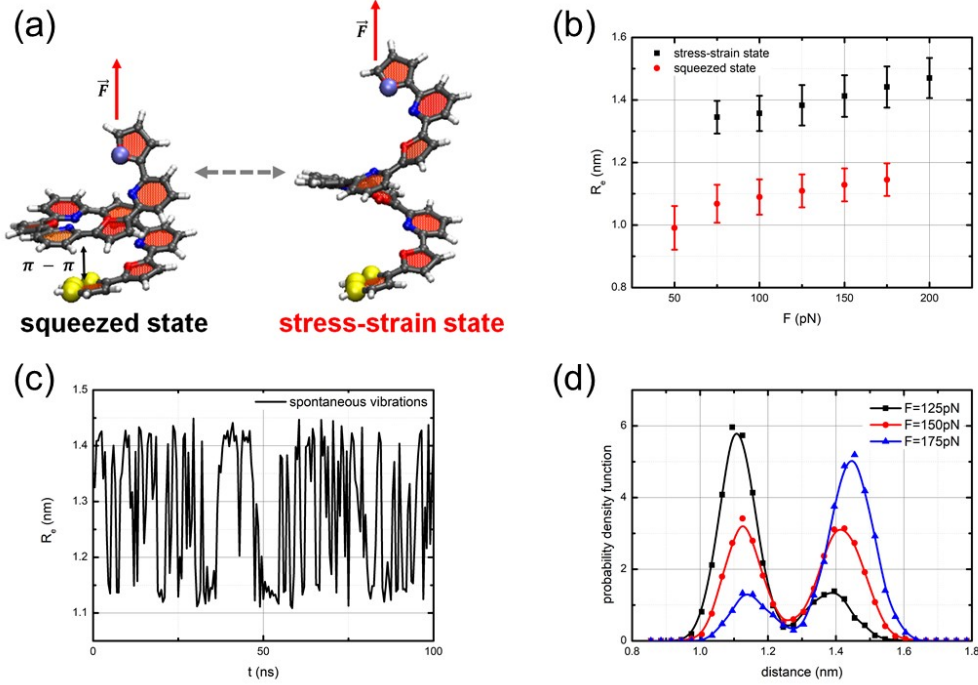


Figure 4: (a) Computational models of the oligo-PF-5 system with applied longitudinal load. The squeezed and the stress-strain states of the spring are shown on the left and right, respectively. The yellow spheres at the lower end of the spring indicate the fixation of the pyridine ring by rigid harmonic force. The pulling force,  $F$ , is applied to the top end of the spring. (b) The state diagram shows a linear elasticity of oligo-PF-5 spring up to  $F \approx 50$  pN and bistability of the spring in the region from  $F \approx 50 - 200$  pN; (c) Spontaneous vibrations of the oligo-PF-5 spring at  $F \approx 150$  pN; (d) Evolution of the probability density for the squeezed and stress-strain states when pulling force surpasses the critical value.

$F = 125 - 175$  pN, both the squeezed and stress-strain states are almost equally visited, signifying that the bistability of the oligo-PF-5 spring becomes approximately symmetrical at a considerable distance from the critical point.

In this region, the spontaneous vibrations of the oligo-PF-5 spring are most prominent. The mean lifetimes of the squeezed and stress-strain states in the spontaneous vibration mode differed in the bistability region, ranging from  $\tau = 1$  ns  $- 3$  ns, depending on the pulling force. In the symmetrical bistability region, neither the squeezed state nor the stress-strain state dominates, resulting in the mean lifetimes of the two states being approximately equal to  $\tau = 2.04$  ns. Utilizing Kramer's rate approximation with a collision time for random perturbations ranging from  $0.1 - 10$  ps, we can roughly estimate the bistability barrier of the oligo-PF-5 spring as  $10 k_B T$ . Again, the bistability barrier of this bistable oligomeric system is approximately ten times greater than the characteristic scale of thermal fluctuations,  $k_B T$ .

Figure 4c) displays a typical trajectory of the long-term dynamics  $R_e(t)$  of the oligo-PF-5 spring within the symmetric bistability region. Clear spontaneous vibrations of the spring can be observed without any additional random perturbations applied to activate them. Instead, these vibrations are solely activated by thermal-bath fluctuations. On the other hand, outside the bistability region, non-vibrating trajectories are prevalent.

To investigate the stochastic resonance mode of the oligo-PF-5 spring, we introduced an additional weak oscillating force by applying an oscillating electrical field,  $E = E_0 \cos(2\pi\nu t)$ , to a unit charge located on the pulling end of the spring. A compensative charge was placed on the fixed end to balance the system (for more details, refer to the "Parameters of periodic signal" section in the Supporting Information). Similar to the oligo-PP-5 spring, the adding of a charge and a fixed counterion significantly shifts the bistability region - for this particular configuration, system exhibits spontaneous vibrations with symmetrical distribution at  $F = 15$  pN. Figure 5a) presents typical vibrations of the end-to-end distance of the oligo-PF-5 spring in the stochastic resonance mode, along with the power spectrum of these vibrations.

The primary resonance peak was observed at a frequency of  $\nu = 1/2\tau$ , where the period of the applied oscillating field was equal to twice the mean lifetime of the states in the spontaneous vibration mode. We extensively scanned a wide

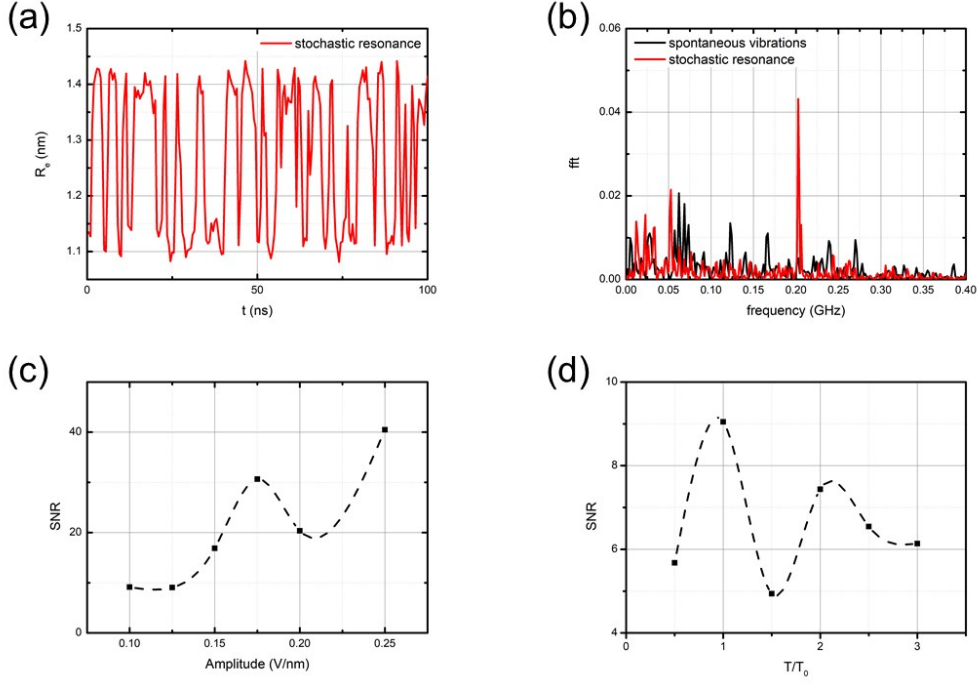


Figure 5: Stochastic resonance of the oligo-PF-5 induces by an oscillating field  $E = E_0 \cos(2\pi\nu t) = E_0 \cos(2\pi t/T)$ : (a) The dynamic trajectory at  $F = 15$  pN,  $T = 4.9$  ns, and  $E_0 = 0.175$  V nm $^{-1}$ ; (b) Power spectrum of spontaneous vibrations (red curve) and stochastic resonance (black curve); (c) The dependence of the main resonance peak amplitude on  $E_0$  ( $T_0 = 4.9$  ns); (d) The dependence of the main resonance peak amplitude on the period  $T$  of oscillating field ( $E_0 = 0.175$  V nm $^{-1}$ ).

range of oscillating fields to identify the maximal resonance response, as determined by the spectral component at the resonance frequency. Figure 5c-d) presents the corresponding results. The maximum resonance response was observed when the period of the oscillating field was close to twice the mean lifetime of the states in the spontaneous vibration mode. In terms of the amplitude of the oscillating field, the maximum resonance occurred at  $E_0 = 0.175$  V nm $^{-1}$ . Notably, the resonance response was diminished in the symmetric bistability region at  $F = 15$  pN. Beyond this region, the lifetimes of the squeezed and stress-strain states became substantially different, rendering the average lifetime less indicative of the resonance frequency.

## 4 Discussion

The main finding of this work is that spontaneous vibrations and stochastic resonance are not exclusive for oligo-PF springs in water[31], but are present in various compounds and observed in different solvents. However, these bistability effects might vary for different systems; such variations are discussed below.

First note concerns the oligo-PF-5 solvated in tetrahydrofuran. In such system, both spontaneous vibrations and stochastic resonance occur at lesser forces than in water. While in case of water the spring's bistability is observed in the region from  $F \approx 240 - 320$  pN and the squeezed and the stress-strain states were almost equally visited in the region from  $F = 270 - 290$  pN, in THF the oligo-PF-5 exhibits spontaneous vibrations in the region from  $F \approx 50 - 200$  pN. Symmetric bistability is achieved at  $F = 150$  pN. If we assume that stacking interaction between the turn and the fixed end of the oligo-PF-5 spring governs its elasticity at low tensiles while at high tensiles the elasticity imposed by oligomeric backbone becomes dominant, then we must suppose that the  $\pi$ -stacking is destroyed later in water. Such difference can be explained by the fact that oligo-PF springs are hydrophobic and prefer to remain in squeezed state in hydrophilic environment.

Second note concerns the overstretching limit of the oligo-PF-5. Our previous findings show that the overstretching of the oligo-PF-5 springs in THF or vacuum occurs at  $F = 275$  pN while in water it happens at  $F = 330$  pN (see Avetisov et al., Figure S3 of the Supplementary Materials). Moreover, at  $F = 330$  pN all three states, the squeezed, the stress-strain and the overstretched, coexist, so one might assume that the bistability region extends up to the

overstretching limit. However, our results of modeling of the oligo-PF-5 in THF do not support this idea: the bistability ceases at  $F = 200$  pN and at larger forces the spring exists at the stress-strain state up to the overstretching limit.

Next note concerns the bistability of the oligo-PP-5. For this system we observe spontaneous vibrations in the region from  $F \approx 30 - 80$  pN and the symmetric bistability is achieved at  $F = 75$  pN. Again, above the force of  $F = 80$  pN the oligo-PP-5 spring exists in stress-strain state up to overstretching limit, which was  $F = 305$  pN in this case. Interestingly enough, we could not detect the bistable behaviour of the oligo-PP-5 in water (See "Oligo-PP-5 in water" section of the Supporting Information). This might be due to the fact that although the bistable behavior of the oligo-PP-5 might be theoretically expected, the overstretching occurred earlier than the transition from its squeezed state to the stress-strain state since these two phenomena are independent from each other. These three observations once again support the idea that the interplay between short-ranged ( $\pi$ -stacking, for instance) and long-ranged couplings is crucial for the observation of the bistable behaviour. Fine tuning of the setup might be required whether one desires to reproduce these results experimentally.

The last note concerns the stochastic resonance of both oligo-PF-5 and oligo-PP-5 springs. If an external oscillating force is strong enough, the forced oscillations of the spring might also happen. These forced oscillations have different origin than the stochastic resonance, the frequency of which is governed by the lifetime of the states in the spontaneous vibrations regime. It is important to distinguish between forced oscillations occurring at large amplitudes of the oscillating field and stochastic resonance observed at weak amplitudes. Based on our results, we determine  $E_0 = 0.175$  V nm<sup>-1</sup> as the limit of the amplitude; below this limit the stochastic resonance was established.

## 5 Conclusion

We conducted atomic level simulations on short PP- and PF-springs under stretching conditions, and the results revealed clear indications of bistable dynamics characteristic of Duffing oscillators. During the study, we fixed one end of the springs while pulling the other end along the spring's axis. We observed typical bistability characteristics, such as spontaneous vibrations and stochastic resonance, in both springs. To explore the symmetrical bistability conditions thoroughly, we examined a wide range of controlling parameters and determined the mean lifetime of the states in the spontaneous vibration mode for each spring.

By using Kramer's rate approximation with collision times ranging from 0.1 to 20 ps, we estimated the bistability barriers for both springs to be within the range of 5 to  $15k_B T$ . Remarkably, the time scales of spontaneous vibrations and the bistability barriers for the oligo-PP-5 and oligo-PF-5 springs were found to be similar to those of the oligomeric Duffing oscillator and oligomeric Euler arch, as described in previous studies[29, 30, 31]. The high bistability barriers of these short oligomeric springs effectively prevent separation of the two states due to thermal noise. However, at the same time, these barriers allow transitions between the states to be activated by thermally enriched fluctuations with higher energy.

Based on our modeling of short PP- and PF-springs, along with the previous modeling of oligomeric Euler arches, we propose that nano-sized oligomeric structures stabilized by short-range, low-energy couplings (e.g., weak hydrogen bonds, hydrophilic-hydrophobic interactions, and  $\pi - \pi$  interactions) can indeed exhibit bistability, accompanied by thermally-activated spontaneous vibrations and stochastic resonance.

## Funding

The authors acknowledge the financial support of the Design Center for Molecular Machines, Moscow, Russia, under the Business Contract 28/11-XΦ-28.11.2022 with N. N. Semenov Federal Research Center for Chemical Physics, Russian Academy of Sciences.

## Acknowledgments

We thank Vladimir Bochenkov, Dmitry Pergushov and Anna Popinako for helpful discussions.

## References

- [1] Alexis Peschot, Chuang Qian, and Tsu-Jae King Liu. Nanoelectromechanical switches for low-power digital computing. *Micromachines*, 6(8):1046–1065, 2015.
- [2] Shaji Varghese, Johannes A. A. W. Elemans, Alan E. Rowan, and Roeland J. M. Nolte. Molecular computing: paths to chemical turing machines. *Chem. Sci.*, 6:6050–6058, 2015.

- [3] Sundus Erbas-Cakmak, Safacan Kolemen, Adam C. Sedgwick, Thorfinnur Gunnlaugsson, Tony D. James, Juyoung Yoon, and Engin U. Akkaya. Molecular logic gates: the past, present and future. *Chem. Soc. Rev.*, 47:2228–2248, 2018.
- [4] Lorient Benda, Benjamin Doistau, Caroline Rossi-Gendron, Lise-Marie Chamoreau, Bernold Hasenknopf, and Guillaume Vives. Substrate-dependent allosteric regulation by switchable catalytic molecular tweezers. *Communications Chemistry*, 2(1):1–11, 2019.
- [5] Guilherme B. Berselli, Aurélien V. Gimenez, Alexandra O’Connor, and Tia E. Keyes. Robust Photoelectric Biomolecular Switch at a Microcavity-Supported Lipid Bilayer. *ACS Applied Materials & Interfaces*, 13(24): 29158–29169, 2021.
- [6] Federico Nicoli, Erica Paltrinieri, Marina Tranfić Bakić, Massimo Baroncini, Serena Silvi, and Alberto Credi. Binary logic operations with artificial molecular machines. *Coordination Chemistry Reviews*, 428:213589, 2021.
- [7] Liang Zhang, Vanesa Marcos, and David A. Leigh. Molecular machines with bio-inspired mechanisms. *Proceedings of the National Academy of Sciences*, 115(38):9397–9404, 2018.
- [8] Tong Shu, Qiming Shen, Xueji Zhang, and Michael J. Serpe. Stimuli-responsive polymer/nanomaterial hybrids for sensing applications. *Analyst*, 145(17):5713–5724, 2020.
- [9] Max C. Lemme, Stefan Wagner, Kangho Lee, Xuge Fan, Gerard J. Verbiest, Sebastian Wittmann, Sebastian Lukas, Robin J. Dolleman, Frank Niklaus, Herre S. J. van der Zant, Georg S. Duesberg, and Peter G. Steeneken. Nanoelectromechanical Sensors Based on Suspended 2D Materials. *Research*, 2020, 2020.
- [10] Zhao-Tao Shi, Qi Zhang, He Tian, and Da-Hui Qu. Driving Smart Molecular Systems by Artificial Molecular Machines. *Advanced Intelligent Systems*, 2(5):1900169, 2020.
- [11] Ivan Aprahamian. The Future of Molecular Machines. *ACS Central Science*, 6(3):347–358, 2020.
- [12] Huidong Li, Chuan Tian, and Z. Daniel Deng. Energy harvesting from low frequency applications using piezoelectric materials. *Applied Physics Reviews*, 1(4):041301, 2014.
- [13] Shi Hyeong Kim, Márcio D. Lima, Mikhail E. Kozlov, Carter S. Haines, Geoffrey M. Spinks, Shazed Aziz, Changsoo Choi, Hyeon Jun Sim, Xuemin Wang, Hongbing Lu, Dong Qian, John D. W. Madden, Ray H. Baughman, and Seon Jeong Kim. Harvesting temperature fluctuations as electrical energy using torsional and tensile polymer muscles. *Energy & Environmental Science*, 8(11):3336–3344, 2015.
- [14] M. L. Ackerman, P. Kumar, M. Neek-Amal, P. M. Thibado, F. M. Peeters, and Surendra Singh. Anomalous Dynamical Behavior of Freestanding Graphene Membranes. *Physical Review Letters*, 117(12):126801, 2016.
- [15] C. Dutreix, R. Avriker, B. Lounis, and F. Pistolesi. Two-level system as topological actuator for nanomechanical modes. *Physical Review Research*, 2(2):023268, 2020.
- [16] P. M. Thibado, P. Kumar, Surendra Singh, M. Ruiz-Garcia, A. Lasanta, and L. L. Bonilla. Fluctuation-induced current from freestanding graphene. *Physical Review E*, 102(4):042101, 2020.
- [17] Denis J. Evans and Debra J. Searles. The Fluctuation Theorem. *Advances in Physics*, 51(7):1529–1585, 2002.
- [18] Udo Seifert. Stochastic thermodynamics, fluctuation theorems and molecular machines. *Reports on Progress in Physics*, 75(12):126001, 2012.
- [19] Jordan M. Horowitz and Todd R. Gingrich. Thermodynamic uncertainty relations constrain non-equilibrium fluctuations. *Nature Physics*, 16(1):15–20, 2020.
- [20] S. Ciliberto. Experiments in Stochastic Thermodynamics: Short History and Perspectives. *Physical Review X*, 7: 021051, 2017.
- [21] G. M. Wang, E. M. Seveick, Emil Mittag, Debra J. Searles, and Denis J. Evans. Experimental Demonstration of Violations of the Second Law of Thermodynamics for Small Systems and Short Time Scales. *Physical Review Letters*, 89(5):050601, 2002.
- [22] P. Jop, A. Petrosyan, and S. Ciliberto. Work and dissipation fluctuations near the stochastic resonance of a colloidal particle. *EPL (Europhysics Letters)*, 81(5):50005, 2008.
- [23] R. D. Astumian. Stochastic pumping of non-equilibrium steady-states: how molecules adapt to a fluctuating environment. *Chemical Communications*, 54(5):427–444, 2018.
- [24] Hadrien Vroylandt, Massimiliano Esposito, and Gatien Verley. Efficiency Fluctuations of Stochastic Machines Undergoing a Phase Transition. *Physical Review Letters*, 124(25):250603, 2020.
- [25] Vladimir Igorevich Arnold. *Catastrophe Theory*. Springer Berlin Heidelberg, Berlin, Heidelberg, 1984. ISBN 9783540128595 9783642967993.

- [26] T. Poston and Ian Stewart. *Catastrophe theory and its applications*. Dover Publications, Mineola, N.Y, 1996. ISBN 9780486692715.
- [27] Georg Duffing. *Erzwungene schwingungen bei veränderlicher eigenfrequenz und ihre technische bedeutung*. Number 41–42. F. Vieweg & sohn, 1918.
- [28] The Duffing Oscillator. In Hans Jürgen Korsch, Hans-Jörg Jodl, and Timo Hartmann, editors, *Chaos: A Program Collection for the PC*, pages 157–184. Springer, Berlin, Heidelberg, 2008. ISBN 9783540748670.
- [29] Vladik A Avetisov, Anastasia A Markina, and Alexander F Valov. Oligomeric “catastrophe machines” with thermally activated bistability and stochastic resonance. *The Journal of Physical Chemistry Letters*, 10(17): 5189–5192, 2019.
- [30] Anastasia Markina, Alexander Muratov, Vladislav Petrovskyy, and Vladik Avetisov. Detection of single molecules using stochastic resonance of bistable oligomers. *Nanomaterials*, 10(12):2519, 2020.
- [31] Vladik A. Avetisov, Maria A. Frolkina, Anastasia A. Markina, Alexander D. Muratov, and Vladislav S. Petrovskii. Short pyridine-furan springs exhibit bistable dynamics of duffing oscillators. *Nanomaterials*, 11(12), 2021.
- [32] H.A. Kramers. Brownian motion in a field of force and the diffusion model of chemical reactions. *Physica*, 7(4): 284–304, 1940.
- [33] R Benzi, A Sutera, and A Vulpiani. The mechanism of stochastic resonance. *Journal of Physics A: Mathematical and General*, 14(11):L453–L457, 1981.
- [34] Roberto Benzi, Giorgio Parisi, Alfonso Sutera, and Angelo Vulpiani. Stochastic resonance in climatic change. *Tellus*, 34(1):10–15, 1982.
- [35] Roberto Benzi, Giorgio Parisi, Alfonso Sutera, and Angelo Vulpiani. A Theory of Stochastic Resonance in Climatic Change. *SIAM Journal on Applied Mathematics*, 43(3):565–578, 1983.
- [36] Luca Gammaitoni, Peter Hänggi, Peter Jung, and Fabio Marchesoni. Stochastic resonance. *Reviews of Modern Physics*, 70(1):223–287, 1998.
- [37] Thomas Wellens, Vyacheslav Shatokhin, and Andreas Buchleitner. Stochastic resonance. *Reports on Progress in Physics*, 67(1):45–105, 2004.
- [38] Ray H Baughman, Changxing Cui, Anvar A Zakhidov, Zafar Iqbal, Joseph N Barisci, Geoff M Spinks, Gordon G Wallace, Alberto Mazzoldi, Danilo De Rossi, Andrew G Rinzier, et al. Carbon nanotube actuators. *Science*, 284 (5418):1340–1344, 1999.
- [39] Hayato Fujii, Agung Setiadi, Yuji Kuwahara, and Megumi Akai-Kasaya. Single walled carbon nanotube-based stochastic resonance device with molecular self-noise source. *Applied Physics Letters*, 111(13):133501, 2017.
- [40] Kun Huang, Shuzhu Zhang, Jinhai Li, and Ze Li. Nonlocal nonlinear model of Bernoulli–Euler nanobeam with small initial curvature and its application to single-walled carbon nanotubes. *Microsystem Technologies*, 25(11): 4303–4310, 2019.
- [41] Jiajie Liang, Lu Huang, Na Li, Yi Huang, Yingpeng Wu, Shaoli Fang, Jiyoung Oh, Mikhail Kozlov, Yanfeng Ma, Feifei Li, et al. Electromechanical actuator with controllable motion, fast response rate, and high-frequency resonance based on graphene and polydiacetylene. *ACS nano*, 6(5):4508–4519, 2012.
- [42] Nuria Forns, Sara de Lorenzo, Maria Manosas, Kumiko Hayashi, Josep Maria Huguet, and Felix Ritort. Improving signal/noise resolution in single-molecule experiments using molecular constructs with short handles. *Biophysical Journal*, 100(7):1765–1774, 2011.
- [43] K Hayashi, S de Lorenzo, M Manosas, JM Huguet, and F Ritort. Single-molecule stochastic resonance. *Physical Review X*, 2(3):031012, 2012.
- [44] Ciro Cecconi, Elizabeth A Shank, Carlos Bustamante, and Susan Marqusee. Direct observation of the three-state folding of a single protein molecule. *Science*, 309(5743):2057–2060, 2005.
- [45] Zhi-hui Lai and Yong-gang Leng. Weak-signal detection based on the stochastic resonance of bistable duffing oscillator and its application in incipient fault diagnosis. *Mechanical Systems and Signal Processing*, 81:60–74, 2016.
- [46] Ze-Qi Lu, Dao Wu, Hu Ding, and Li-Qun Chen. Vibration isolation and energy harvesting integrated in a stewart platform with high static and low dynamic stiffness. *Applied Mathematical Modelling*, 89:249–267, 2021.
- [47] R. Alan Jones, Marielena Karatza, Tevita N. Voro, Pervin U. Civeir, Annete Franck, Orhan Ozturk, John P. Seaman, Alexander P. Whitmore, and David J. Williamson. Extended heterocyclic systems 1. the synthesis and characterisation of pyrrolylpyridines, alternating pyrrole: Pyridine oligomers and polymers, and related systems. *Tetrahedron*, 52(26):8707–8724, 1996.

- [48] R. Alan Jones and Pervin U. Civcir. Extended heterocyclic systems 2. the synthesis and characterisation of (2-furyl) pyridines, (2-thienyl) pyridines, and furan-pyridine and thiophene-pyridine oligomers. *Tetrahedron*, 53(34):11529–11540, 1997.
- [49] Harikrishna Sahu, Shashwat Gupta, Priyank Gaur, and Aditya N. Panda. Structure and optoelectronic properties of helical pyridine–furan, pyridine–pyrrole and pyridine–thiophene oligomers. *Physical Chemistry Chemical Physics*, 17(32):20647–20657, 2015.
- [50] Mark James Abraham, Teemu Murtola, Roland Schulz, Szilárd Páll, Jeremy C Smith, Berk Hess, and Erik Lindahl. Gromacs: High performance molecular simulations through multi-level parallelism from laptops to supercomputers. *SoftwareX*, 1:19–25, 2015.
- [51] George A Kaminski, Richard A Friesner, Julian Tirado-Rives, and William L Jorgensen. Evaluation and reparametrization of the op1s-aa force field for proteins via comparison with accurate quantum chemical calculations on peptides. *The Journal of Physical Chemistry B*, 105(28):6474–6487, 2001.
- [52] Giovanni Bussi, Davide Donadio, and Michele Parrinello. Canonical sampling through velocity rescaling. *The Journal of Chemical Physics*, 126(1):014101, 2007.